Hindawi
Advances in Materials Science and Engineering
Volume 2024, Article ID 4275035, 11 pages
https://doi.org/10.1155/2024/4275035

Research Article

Effect of Codoping Zinc Oxide Nanoparticles with Sulfur and Nitrogen on Its Energy Bandgap, Antioxidant Properties, and Antibacterial Activity

Diriba Yadesa, Jabessa Nagasa Guyasa, and Tamene Tadesse Beyene

Department of Chemistry, College of Natural Sciences, Jimma University, P.O. Box 378, Jimma, Ethiopia

Correspondence should be addressed to Tamene Tadesse Beyene; tamene.tadesse@ju.edu.et

Received 9 November 2023; Revised 5 February 2024; Accepted 22 February 2024; Published 26 February 2024

Academic Editor: Samia A. Gad

Zinc oxide nanoparticles (ZnO-NPs) are used in various fields such as industrial, environmental remediation, catalytic, and antibacterial applications. However, their ability to absorb visible light is limited due to their high-energy bandgap and fast electron-hole recombination, which restricts their use. To enhance the efficiency of ZnO-NPs in medical and other applications, surface functionality can be modified through doping. Here, we investigated the effects of S and N doping on the energy bandgap of ZnO-NP and their antimicrobial and antioxidant activities. The results showed that the optical bandgap energy of pure ZnO-NPs was 2.98 eV while that of 6% N-ZnO, 4% S-ZnO, and S4-N6-ZnO was 2.78, 2.69, and 2.63 eV, respectively. The energy bandgap reduction is attributed to the changes in the electronic level of zinc oxide as the result of doping. The crystal size of pure ZnO-NPs, 6% N-ZnO, 4% S-ZnO, and S4-N6-ZnO was 29.06, 27.05, 29.02, and 25.06 nm, respectively, as calculated from XRD data using FWHM. Following the bandgap and particle size reduction, the antimicrobial activities of the dual-doped ZnO-NPs surpassed that of the pure ZnO-NPs. Moreover, dual doping improved the antioxidant activity of ZnO-NPs from 52.45% to 88.89% for the optimized concentration. Therefore, incorporating S and N as dual dopants can enhance the functionality and efficiency of ZnO-NPs in various fields.

1. Introduction

Nanotechnology studies materials at the nanoscale of 1–100 nm. It is an interdisciplinary field that has opened up new opportunities in material science and engineering [1–3]. Metal oxide nanoparticles (MONPs) have several uses, including catalysis [4], optoelectronic materials [4], sensors [5], and environmental remediation [6]. Due to their high surface area, nanoparticles are potentially valuable in biomedical applications since they can produce reactive oxygen species (ROS) more effectively. ROS production can be influenced by exposure to ultraviolet (UV) light, disruption of intracellular metabolic activities, and antioxidant systems. As a result, oxidative stress can occur in cells, leading to damage to DNA, cell membranes, proteins, and even cell death [7–10].

Some commonly used metal oxide nanoparticles (MONPs) include Ag_2O, CuO, ZnO, TiO_2, Al_2O_3, CrO_2 and NiO [11, 12]. Among these, zinc oxide nanoparticles (ZnO-NPs) have gained significant attention from researchers due to their low toxicity, biodegradability, affordability, and therapeutic and diagnostic potentials [6, 9, 13]. These nanoparticles find a wide range of applications in medicine, packaging, photocatalysis, and as antibacterial agents. ZnO-NPs have been proven safe for use in these applications, as they can easily diffuse into the food material, kill microbes, and prevent humans from falling ill [14, 15]. Moreover, ZnO has been found to significantly enhance the degradation of tenacious dyes that cause harmful environmental pollution. However, the wide bandgap of ZnO (3.37 eV) [9, 16–18], its large exaction binding energy of 60 meV [14, 19, 20], and its tendency to agglomerate [21–23] have limited its potential applications.

To address these issues, researchers have explored various approaches to modify ZnO-NPs' properties. One such

approach is doping, which involves the intentional introduction of impurities into a crystal lattice [6, 9, 24–26]. Dual doping is a promising technique that can enhance a limited portion of sunlight and improve the optical properties of ZnO-NPs. Doping can also minimize the energy bandgap, thereby enhancing ZnO's antioxidant and antimicrobial properties [14, 26–28]. The introduction of a limited amount of foreign materials, such as biomolecules and transition metals (Mn, Fe, Cr, and Cu) at the nanoscale, can increase and modify the surface area of ZnO-NPs, improving their functionality and efficiency [5, 6, 9, 29]. Doping does not alter the precursor material but instead introduces new functionalities [9, 18]. Besides doping, the physical and chemical behavior of ZnO-NPs can be modified by altering their shape using various methods and materials for synthesis [30].

ZnO nanocomposites are a better option than bare ZnO nanoparticles since they have improved properties [31, 32]. Nanocomposite materials have separate properties such as mechanical [33], electrical [34], optical [35], chemical [36], and catalytic properties [6, 32]. Nanoparticles have certain advantages over their counterparts, making them more favorable. The Food and Drug Administration considers ZnO to be a safe material for biomedical applications, including drug delivery systems [37]. ZnO nanoparticles have been used effectively in tissue engineering (TE) applications [32] with various shapes such as nanoflower (NF) [13] and nanowires (NW) [34, 38]. In addition, several cell lines have shown better adhesion, growth, and differentiation on these surfaces [39].

This study explores the impact of S and N codoping on the energy bandgap and antimicrobial activity of ZnO-NPs. Researchers have previously reported that the addition of sulfur to ZnO-NPs at varying temperatures reduces the bandgap energy from 3.34 to 3.22 eV [6, 9, 18]. Similarly, Ag-N-codoped ZnO-NPs have been studied for their effects on the energy bandgap and photocatalytic degradation of organic pollutants by various authors [39–41]. However, no prior research has investigated the impact of S-N-codoping on the energy band and its antimicrobial activity.

The present study focuses on the dual nonmetal codoping of ZnO-NPs with S and N to minimize the energy bandgap and enhance their antimicrobial and antioxidant activity. The dual-doped ZnO-NPs exhibit improved physicochemical properties, with their UV-vis absorbance wavelength shifting towards the red region, resulting in a reduced energy bandgap from 2.93 eV to 2.63 eV. The dual-doped nanoparticles also demonstrate stronger antioxidant and antimicrobial activities than the ZnO-NPs.

2. Materials and Methods

ZnO nanoparticles (NPs) were prepared using the sol-gel method, which provides several benefits, such as repeatability, ease of synthesis, and regulation of composition. To create S- and N-codoped ZnO-NPs, the synthesized ZnO-NPs were mixed with appropriate amounts of urea and ZnS. The main objective of this synthesis was to investigate the effect of doping on the physicochemical properties of ZnO-NPs.

2.1. Chemicals and Instruments. Chemicals such as zinc nitrate dihydrate ($Zn(NO_3)_2).2H_2O \geq 98\%$, Loba Chemie Pvt. Ltd), sodium hydroxide ($NaOH) \geq 98\%$, Blulux Laboratories Ltd., 121005), ethanol (C_2H_5OH), 99.9%, Favor Trading Co. PLC), citric acid ($HOC(COOH)(CH_2COOH)_2$) (≥99%, Loba Chemie Pvt. Ltd.), urea (NH_2CONH_2, Blulux Laboratories Ltd., 121005), and double-distilled water were used in this research work.

In this study, various types of laboratory equipment were used including beakers, measurement cylinders, magnetic stirrers, electronic balances, muffle furnaces, crystallizing dishes, burettes, funnels, filter paper, pH meters, spoons, sample bottles, and pipettes. In addition, advanced analytical instruments were used such as the directed ray radiometer (DRAWELL RADIometer-700), directed ray Cu radiometer (Cu Kα Radiometer ($\lambda = 1.54178$ Å), direct ray visimeter (UV-Vis), and detailed ray spectrometer (Ray Spectrometer-200 PLUS-223E12).

2.2. Synthesis of ZnO-NPs. Zinc oxide nanoparticles were synthesized using sol-gel techniques. The first step involved dissolving 0.4 M of zinc nitrate in 50 mL of distilled water. Next, 0.8 g of NaOH was dissolved in 100 mL of distilled water at room temperature to prepare 2 M sodium hydroxide. Continuous stirring of both solutions was carried out for 30 minutes using a magnetic stirrer. The NaOH solution was then added slowly to the ZnO nitrate solution while stirring continuously, and the pH was adjusted to 10. After cooling for 2 hours, the solution was filtered using Whatman filter paper, washed 3 times with distilled water, and treated with ethanol. The filtered sample was then dried in an oven at 60°C and allowed to cool for 2 hours before being calcined at 500°C in a muffle furnace. The resulting white powders were confirmed to contain ZnO nanoparticles.

2.3. Preparation of N-Doped ZnO-NPs. To select the optimized urea concentration, we dissolved 0.015%, 0.03%, 0.045%, and 0.06 g of urea in 25 mL of distilled water, at room temperature. We then added each concentration of urea to a previously prepared solution of hexahydrated zinc nitrate and stirred for 10 min to obtain a homogeneous solution. To prepare sodium hydroxide (2 M), we dissolved 0.8 g NaOH into 100 mL of distilled water. We then dropwise added the sodium hydroxide to the previously prepared zinc nitrate solution and urea solution, stirring until a precipitate formed. We controlled the pH to 10 and heated the mixture at 60°C, stirring continuously for 2 hours. We kept the solution cool and filtered using Whatman filter paper, which was oven-dried at 60°C and then calcinated in muffle furnaces at 500°C for 2 hours.

2.4. Preparation of S-Doped ZnO NPs. To prepare S-doped ZnO-NPs, first varying amounts of ZnS salt (0.01, 0.02, 0.03, and 0.04 g) were measured and dissolved in 10 mL of distilled water. Next, 1 g of ZnO-NPs was mixed with the ZnS solution after being dissolved in 10 mL of ethanol. The solution was stirred at room temperature for 3 hours. The

S/ZnO mixture was filtered, and the residue was washed with distilled water until the pH of the removed water reached 7. The residue was air-dried overnight and then calcined at 500°C for 2 hours.

2.5. Preparation of S-N-Co-Doped ZnO NPs. S- and N-doped ZnO-NPs were prepared from zinc oxide nanoparticles by dissolving 1 g of ZnO in 10 mL of ethanol and mixing a selected amount (0.04 M) of urea solution and 0.04 M zinc sulfide solution. It was then stirred at room temperature for 3 hours, filtered, washed with distilled water until the pH of the removed water reached 7, left in air overnight, and calcined at 500°C for 2 hours.

2.6. Antioxidant Activity Test. As part of our research, we conducted a 2, 2-diphenyl-1-picrylhydrazyl (DPPH) radical scavenging method to test the effectiveness of ZnO-NPs in scavenging free radicals. The experiment involved observing how a methanol solution of DPPH changes when exposed to NPs. DPPH produces a purple or violet color in methanol, which turns yellow in the presence of antioxidants. We prepared a 0.1 mM DPPH methanol solution and mixed it with 1 mL of methanol solution containing pure ZnO NPS and S- and N-doped ZnO NPs at concentrations of 70, 90, 110, and 130 mg/mL. The mixture was then vortexed and incubated in the dark at room temperature for 30 minutes. We measured the absorbance of the mixture at 517 nm using a spectrophotometer to determine the percentage of DPPH radical scavenging activity. Ascorbic acid was used as a standard.

$$\%\ \text{DPPH radical scavenging activity} = \frac{(A_O - A_1)}{A_0} X100, \tag{1}$$

where the absorbance of the control is A_0 and the absorbance of the sample is A_1.

After plotting the percent of inhibition against concentration, the IC50 was derived from the graph. The experiment was repeated three times at each concentration.

2.7. Antimicrobial Activity. The Department of Biology at Jimma University conducted bacterial studies using the agar disk diffusion method. They tested the synthesized nanoparticles on bacterial strains such as *Staphylococcus aureus*, *Salmonella typhimurium*, *Bacillus cereus*, and *Escherichia coli*. The nanoparticles were also tested for their antifungal activity against *Candida albicans*. For the test, cultures were used to inoculate the medium using test tubes with concentrations or densities approximately equal to 0.5 McFarland standard. Test bacteria and fungi were inoculated with freshly grown liquid cultures similar to 0.5 McFarland turbidity using Mueller–Hinton agar and potato dextrose agar, respectively. DMSO was used as the negative control, and gentamicin and Clo were used as positive controls for bacteria and fungi, respectively. The test compound was dissolved in DMSO solutions containing 100 mg/ml. The solution was then added to the culture wells and incubated at 37°C for 24 hours. The plate had an inhibition zone around a 6 mm diameter plain paper disc, and the antibacterial activity of the nanoparticles was detected by measuring the diameter of the inhibition zone formed around the sample.

3. Results and Discussion

UV-Vis spectroscopic measurements were performed to investigate the effect of doping on the absorption of ZnO-NPs. Here, different amounts of impurities were mixed with pure ZnO-NPs and their characteristic UV-Vis absorption was measured. The introduction of N and S shifted the maximum absorption wavelength towards the red. Among all measurements, 6% N-ZnO, 4% S-ZnO, and S4-N6-ZnO showed the greatest change in UV-Vis absorption and was considered the optimal composition for this study. Figure 1 shows the UV-visible absorption spectra of 6% N-ZnO, 4% S-ZnO, and S4-N6-ZnO. Hybridization of Zn with the HOMO of the highest occupied molecular orbital resulted in the lowest unoccupied molecular orbital (LUMO). The bandgap is due to the 2p orbital and leads to UV-induced absorption. It shows the absorption spectra of all freshly prepared pure-doped and doubly-doped ZnO-NPs. Absorption values of ZnO are observed with other materials at wavelengths of 370 nm, 376 nm, 377 nm, and 379 nm. These apply to 4% S-ZnO, 6% N-ZnO, and S4-N6-ZnO, respectively. There are no other peaks. Only a redshift of ZnO to doped and doubly-doped ZnO-NPs was observed. This indicates that the doping process did not change the crystal structure of ZnO-NPs.

3.1. Optical Bandgap Energy Analysis. The optical energy bandwidth (E_g) was calculated using the Tauc method [42, 43]. A Tauc curve can be plotted using the calculated UV-Vis absorption results using the following equation:

$$(\alpha h\nu)^2 = h\nu - E_g, \tag{2}$$

where α stands for the absorption coefficient, h represents Planck's constant, ν is the frequency of light, and E_g is the optical band gap.

Figure 2 illustrates a Tauc plot plotted between (a) 2 and hv using the equation above, where extrapolating the linear part of the plot gives the bandwidth value. The calculated band values are 2.98 eV, 2.78 eV, 2.69 eV, and 2.63 eV for pure ZnO-NPs, 6% N-ZnO, 4% S-ZnO, and S4-N6-ZnO. As expected, there is a difference in the energy bands of doped and codoped compared to pure ZnO NPs. In particular, the energy bandgap of S4-N6-ZnO decreases compared to the energy bandgap of pure ZnO-NPs, 6% N-ZnO, and 4% S-ZnO. This may be due to changes in the electronic level of zinc oxide. More 2p nitrogen electrons compared to nitrogen-substituted oxygen induce a new energy level between the conduction and valence bands of ZnO, leading to a decrease in the bandgap of ZnO NPs.

3.2. Powder X-Ray Diffraction (XRD) Analysis. The sample was produced using a Zn-$(NO_3)_2.6H_2O$ precursor via a standard sol-gel process and calcined at 500°C for 5 hours. The product was characterized through Cu Kα radiation at

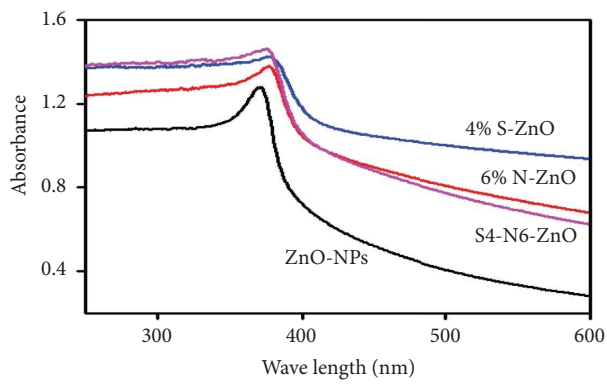

Figure 1: Ultraviolet-visible absorbance spectra of bare, doped, and codoped quantities of nitrogen and sulfur zinc oxides.

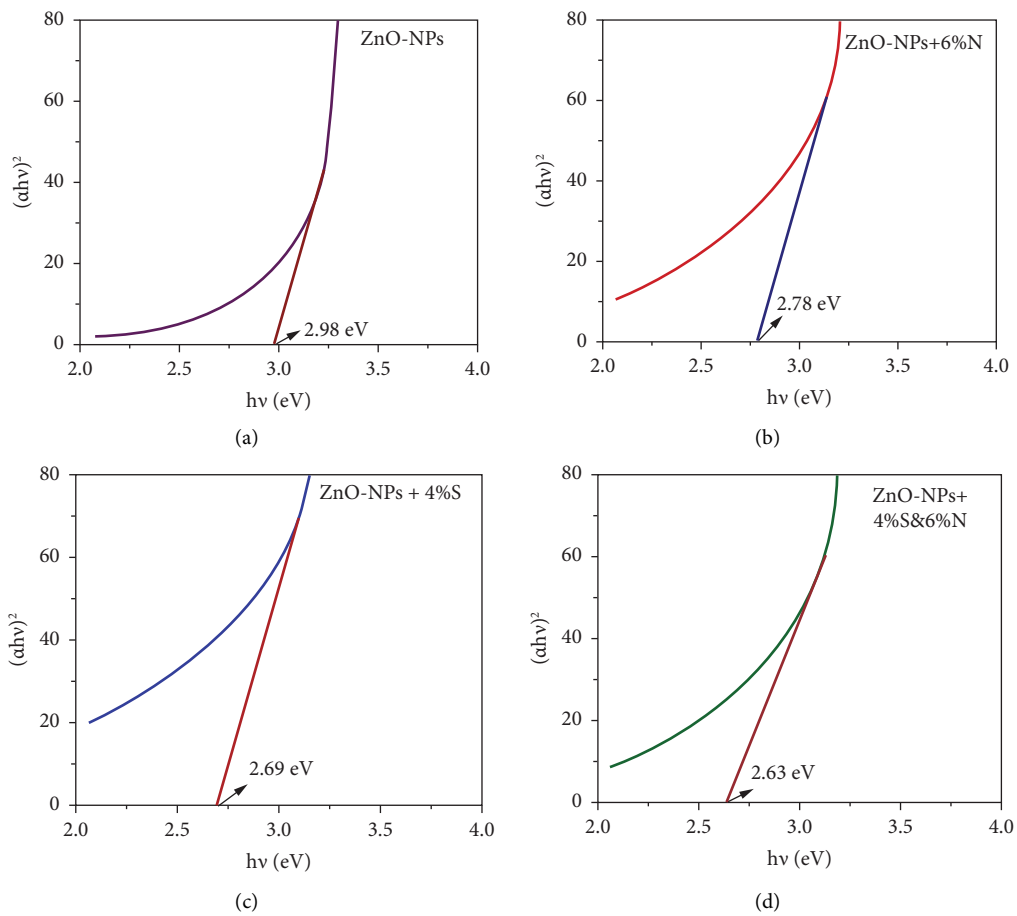

Figure 2: Energy bandgaps of bare, doped, and codoped quantities of nitrogen and sulfur. (a) Pure ZnO-NPs, (b) 6% N-ZnO, (c) 4% S-ZnO, and (d) S4-N6-ZnO.

2θ of 10–80°. The XRD peaks are illustrated in Figure 3, demonstrating a hexagonal crystal structure (JCPDS). The highest peaks were identified at $2\theta = 28.62°$, 31.86°, 34.62°, 36.28°, 47.64°, 56°, 68.18°, 78°, and 78.15°. These lines were identified as the hexagonal phase of ZnO. The particles display high crystallinity at 36.28° for both single and double doping, as indicated by a sharp peak and high intensity. The growth of larger crystals from smaller ones leads to a reduction in the number of smaller grains, whereas larger grains continue to grow.

In Figure 3, we can observe pure (doped), S-doped, and N-doped ZnO-NPs. Specific peaks can be located at 20 (degree) = 28.62°, 31.86°, 34.62°, 36.28°, 47.64°, 56.78°, 63.15°, and 68.18°. The diffraction patterns of S-doped and N-doped ZnO-NP are very similar to those of pure ZnO-NP and are almost identical. This means that sulfur and nitrogen atoms were added to the ZnO crystals. The absence of additional peaks indicates that the presence of sulfur and nitrogen compounds or complexes is excluded from the doped ZnO-NPs with respect to S and N. However, the additional peaks

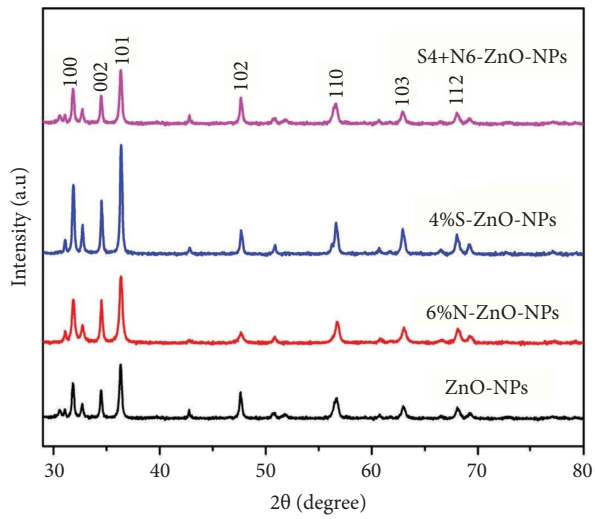

Figure 3: XRD pattern of pure ZnO-NPs, 6% N-ZnO, 4% S-ZnO, and S4-N6-ZnO.

of S-N-coding indicate the presence of residual compounds or complexes of S and N. On the other hand, the intensity of the diffraction peaks changes with the dopant concentration. The decrease in doping intensity is due to the change in electron density. In general, when using double S and N doping, the intensity of the diffraction peaks is significantly reduced compared to single doping. This indicates the relative loss of crystallinity due to changes in the crystal lattice.

The average size of crystallites of ZnO-NPs doped with S, N, and both S and N, as well as those that are pure, can be determined by using the full width at half maximum (FWHM) of the strongest peaks of their respective crystals. The calculation involves using the Dybe–Scherrer equation, which is expressed as $D = (0.9\ \lambda)/\beta\cos\theta$. Here, λ represents the X-ray wavelength, D is the average crystal size, θ is the Bragg diffraction angle, and β is the FWHM in radians. It is observed that the size of crystallites decreases with increasing doping concentration, resulting in a decrease in the peak intensity. The size of the synthesized NPs for the strongest peaks is recorded in Table 1 and is calculated based on XRD results using the Debye–Scherrer equation [6, 9, 43]. The crystallographic size in the decreasing order of the synthesized NPs is as follows: S-ZnO > ZnO NPs > S-N-ZnO > N-ZnO NPs. The lower size of S-N-ZnO and N-ZnO-NPs is due to N doping, as N doping shows the lowest crystallite size (Table 1) [27]. The most notable trend as a function of particle size is that the surface area-to-volume ratio increases for smaller particles. Here, it is worth mentioning that the additional peaks introduced in the XRD patterns could be due to the possible introduction trace amounts of impurities during sample transportation from synthesis laboratory to the XRD characterizations.

3.3. FTIR-Analysis. The transmission properties of bare ZnO nanoparticles, doped ZnO nanoparticles, and codoped ZnO nanoparticles were measured by FTIR in the wave number range of 4000–400 cm^{-1}. Figure 4 shows the IR spectra of ZnO-NPs, 6% N-ZnO, 4% S-ZnO, and S4-N6-ZnO samples, highlighting the differences in functional groups. The IR spectrum reveals that the absorption band of zinc oxide in the Zn-O stretching mode is between 400 and 850 cm^{-1}, corresponding to the hexagonal crystal structure of ZnO [40, 44]. The peak observed between 3300 cm^{-1} and 3500 cm^{-1} represents the O-H stretching mode of hydroxyl groups due to water adsorption on the surface, indicating the presence of impurities mainly near the ZnO surface. Furthermore, a strong absorption peak at 877 cm^{-1} was observed in all samples, which can be attributed to the substitution of H by O. A new peak was observed at 1410 cm^{-1}, which was not sharp due to the formation of the sample microstructure (Zn-S) during the doping process. The peak at 1387 cm^{-1} corresponds to the Zn-N stretching vibration, and the peak at about 2426 cm^{-1} is due to the C=O stretching vibration.

Table 1: Calculated crystalline size of synthesized pure, S-doped, N-doped, and S-N-codoped ZnO-NPs at 500°C.

S/N	Materials	θ	Cos θ	λ (nm)	β (radian)	D (nm)
1	ZnO NPs	18.18	0.78	0.154	0.0039	29.06
2	6% N-ZnO	18.18	0.78	0.154	0.0052	27.05
3	4% S-ZnO	18.18	0.78	0.154	0.0038	29.21
4	S4-N6-ZnO	18.18	0.78	0.154	0.0043	25.06

3.4. Morphological Analysis. To clarify the external structure of 6% N-ZnO, 4% S-ZnO, and S4-N6, SEM analysis was conducted. The SEM images of pure ZnO-NPs, 6% N-ZnO, 4% S-ZnO, and S4-N6 are displayed in Figure 5. The morphology of dual-doped ZnO-NPs (S4-N6) is significantly improved compared to single-doped and pristine ZnO-NPs. The crystal size of pure ZnO-NPs, 6% N-ZnO, 4% S-ZnO, and S4-N6-ZnO are 29.06, 22.44, 29.21, and 25.76 nm, respectively, as calculated from XRD data. There is good agreement between the calculated particle size from the XRD patterns and the morphology of the synthesized materials. It is worth mentioning that adding dopants to pure ZnO-NPs improved stability and morphology by modifying surface characteristics as revealed by the FTIR analysis. As a result of improvement in morphology, several physicochemical properties of the doped nanoparticle were enhanced compared to the pure one.

The antimicrobial exercises of pure ZnO-NPs (undoped), N-doped ZnO-NPs, S-doped ZnO-NPs, and S and N codoped ZnO-NPs against *Staphylococcus aureus*, *Salamonella typhi* (−ve), *Bacillus cereus*, *Escherichia coli* (−ve), and *Candida alibican* were done utilizing the disk dissemination strategy and the chart for the zone of inhibition is demonstrated in Figure 6. The antimicrobial action for pure ZnO-NPs (undoped), 6% N-doped ZnO-NPs, and 4% S-doped ZnO-NPs were found to be compelling against all microscopic organisms' strains and organisms. In any case, the rate decay in S-N-ZnO NPs was found to significantly increment in bacterial action. The antimicrobial impacts are in this way compared to engineered NPs, which were more dynamic for Gram-positive microscopic organisms. The conceivable reason behind contrasts is (i) cell layer structure, (ii) physiology and metabolic exercises of the cell, and (iii)

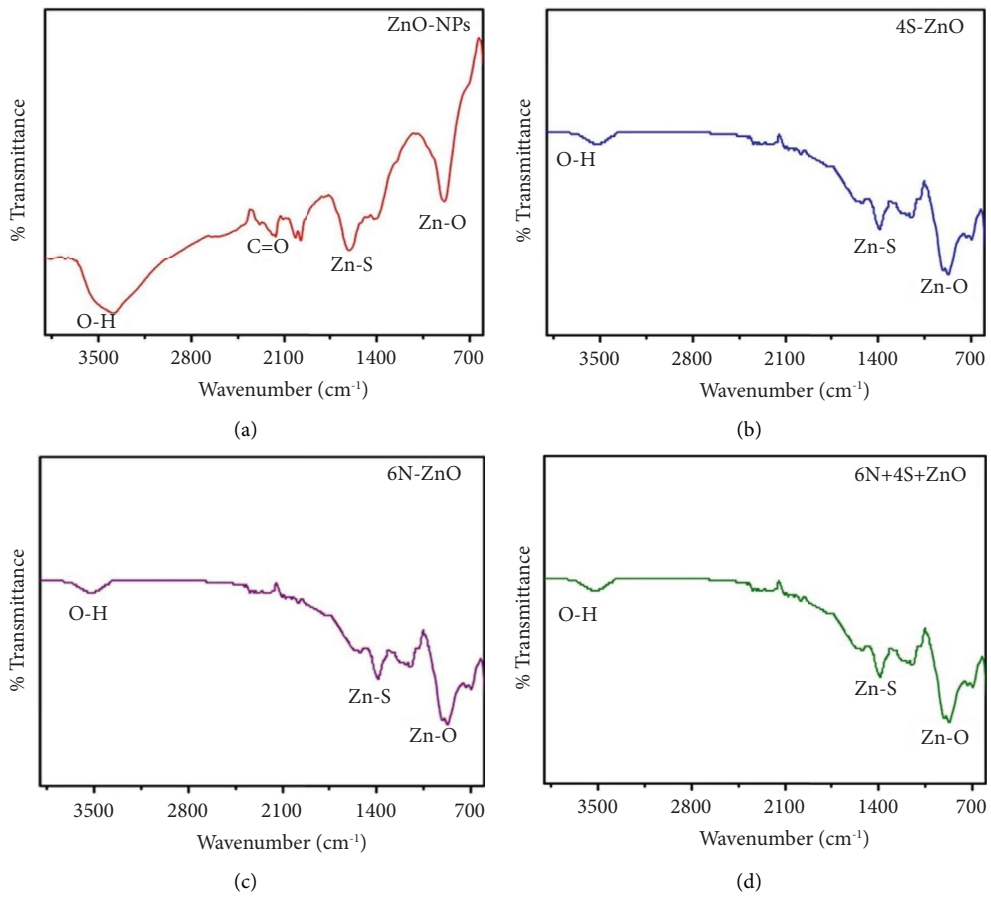

Figure 4: FTIR bands of bare and doped quantities of (a) ZnO-NPs, (b) 4% S-ZnO, (c) 6% N-ZnO, and (d) S4-N6-ZnO.

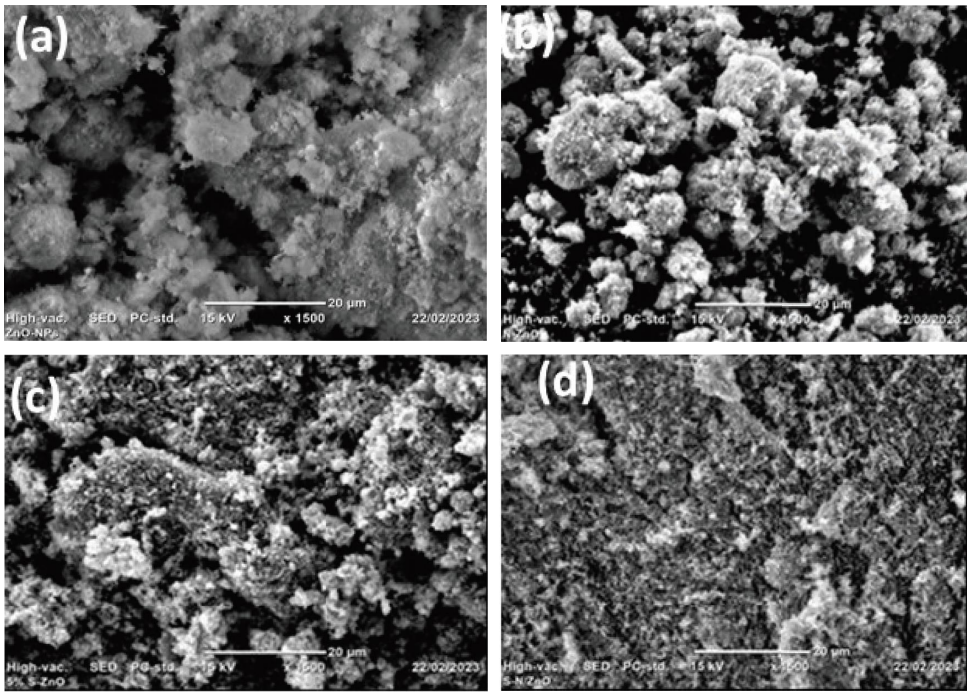

Figure 5: SEM image of (a) pure ZnO-NPs, (b) 6% N-ZnO, (c) 4% S-ZnO, and (d) S4-N6-ZnO.

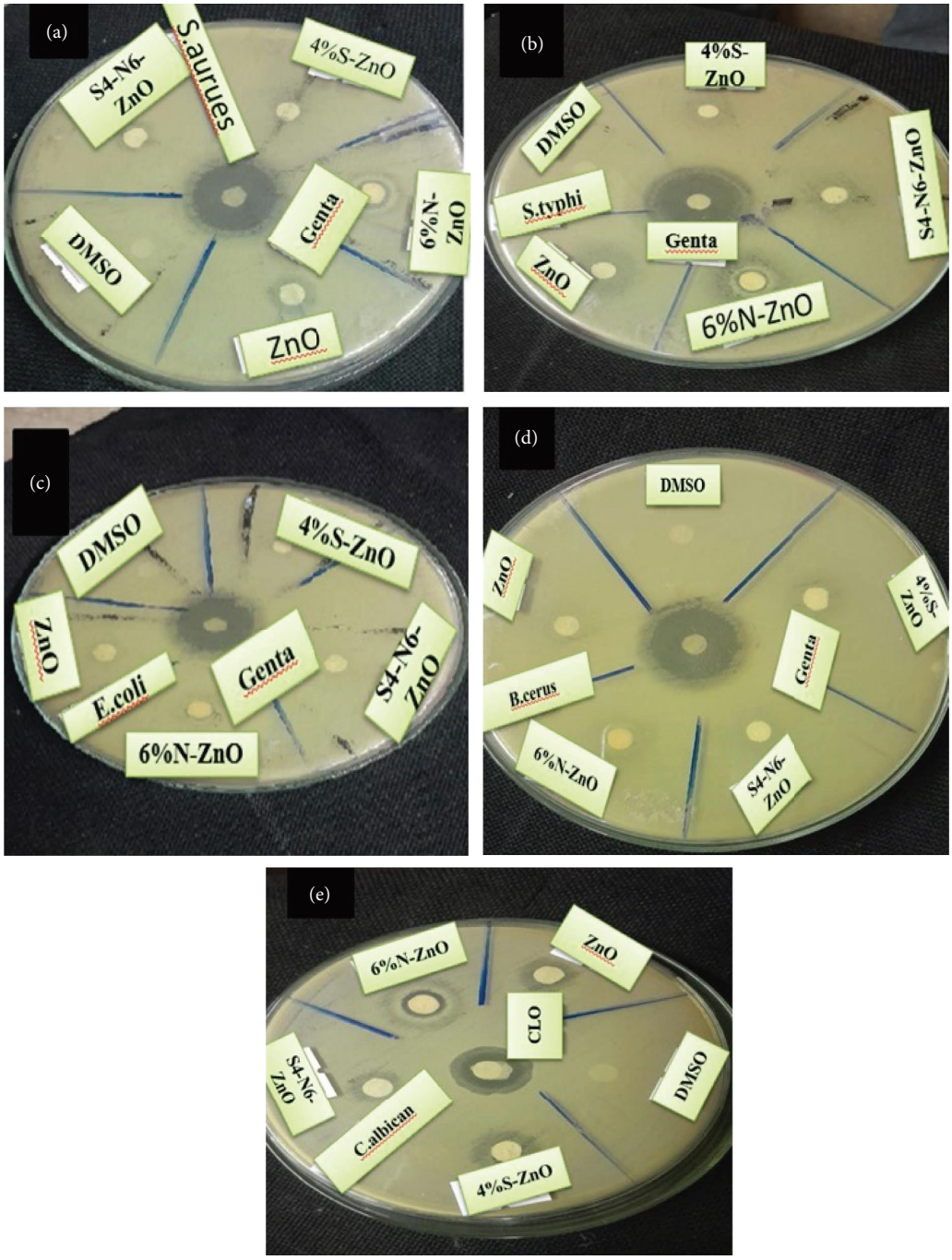

Figure 6: Picture showing the zone of inhibition of the pure and doped ZnO-NPs against some selected microorganisms using Genta and CLO as the positive control and DMSO as the negative control (a) *S. aureus*, (b) *S. Typhi*, (c) *E. coli*, (d) *B. cerus*, and (e) *C. albican*.

degree of contact of Gram-positive and Gram-negative microscopic organisms. The antibacterial movement of single-doped and dual-doped ZnO nanoparticles appeared that they were safer for Gram-negative microbes than that of Gram-positive microbes. For the most part, 6% N-doped ZnO NPs appeared way better antifungal movement when compared with undoped ZnO-NPs, as demonstrated by the inhibition zone in Table 2 and usually upheld in prior writing. The improvement in antimicrobial activity is attributed to the improved stability and reduced particle size due to doping, which enables the particles to penetrate bacterial cell walls easily. This changes the structure of the cytoplasmic membrane, which in turn ruptures organelles and even leads to cell lysis.

3.5. Antioxidant Activity. The scavenging properties of different types of ZnO nanoparticles were evaluated using the DPPH method. The types included pure (undoped) ZnO-NPs, 6% N-doped NPs, 4% S-doped NPs, and S4-N6 ZnO-NPs (Figure 7). The results showed that all types of NPs had an enhanced radical scavenging activity (RSA) with

Table 2: Antibacterial and antifungal activity of ZnO, 6% N-ZnO, 4% S-ZnO, and S4-N6-ZnO.

Name of sample	Zone of inhibition (mm)				
	S. aureus	*S. typhi*	*E. coli*	*B. cerus*	*C. albican*
ZnO	12 ± 0.12	16 ± 0.12	11 ± 0.20	9 ± 0.20	13 ± 0.20
6% N-ZnO	14 ± 0.30	14 ± 0.20	12 ± 0.20	16 ± 0.40	17 ± 0.20
4% S-ZnO	12 ± 0.12	17 ± 0.20	13 ± 0.30	16 ± 0.20	12 ± 0.30
S4-N6-ZnO	19 ± 0.20	16.±0.31	14 ± 0.40	18 ± 0.20	18 ± 0.20
+Ve control(Genta and CLO)	29 ± 0.30	30 ± 0.40	26 ± 0.20	27 ± 0.30	21 ± 0.20
−Ve control (DMSO)	—	—	—	—	—

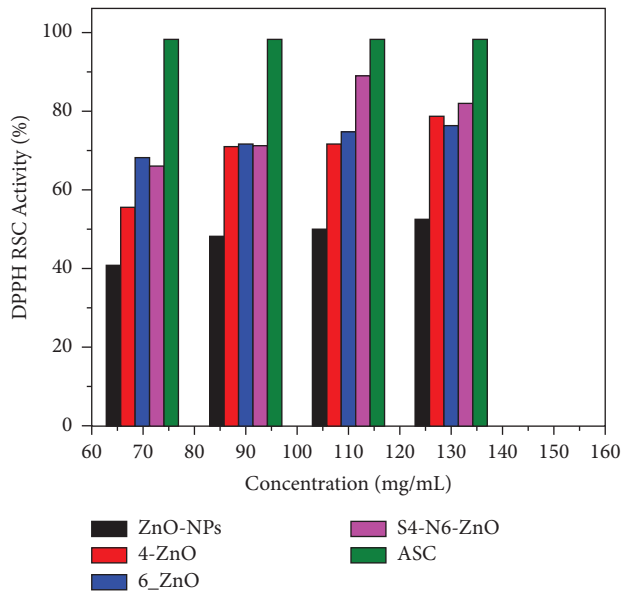

Figure 7: DDPH scavenging activity of ZnO-NPs, 6% N-ZnO, 4% S-ZnO, and S4-N6-ZnO.

Table 3: DDPH radical scavenging assay.

Materials	Concentration (mg/mL)	% RSC of DDPH	IC50 (mg/mL)
ZnO-NPs	70	40.98380181	67.73840609
	90	48.40400191	
	110	50.04764173	
	130	52.45354931	
6% N-ZnO	70	68.16341115	40.19248396
	90	71.59361601	
	110	74.24964269	
	130	76.36969986	
4% S-ZnO	70	55.22868032	27.10025434
	90	71.2720343	
	110	72.43925679	
	130	78.6922344	
S4-N6-ZnO	70	65.895664602	24.40025434
	90	71.20771796	
	110	81.89947594	
	130	88.94949976	
Ascorbic acid	70	97.6680324	43.75954198
	90	98.70152454	
	110	98.8325393	
	130	98.9231062	

increasing nanoparticle concentration. The individual IC50 values of each NP were measured and recorded in Table 3. It is well-known that ZnO-NPs and 6% N-doped NPs have high antioxidant activity, whereas 4% S-doped and codoped NPs reach the break-even point when limited to 50 μg/mL. The exchange of electron thickness from oxygen particles to nitrogen molecules in ZnO-NPs enables them to retain DPPH-free radicals containing odd electrons through $n \longrightarrow \pi$ motion [25]. The increased in the antioxidant activities attributed to the productions species that scavenge the reactive oxygen species and mimic the antioxidant molecule due to their intrinsic physicochemical properties.

4. Conclusion

In this study, we examined the effects of sulfur and nitrogen doping, as well as codoping, on the properties of ZnO nanoparticles. Changes in the optical energy bandgap, antimicrobial activity, and antioxidant activity are examined in the study. For nitrogen and sulfur doping, the UV absorption spectra show a redshift from 370 to 377 nm and 378 nm, respectively, while for S-N-codoping, the shift is from 370 to 379 nm. When nitrogen doping is applied, the gap energy decreases from 2.97 to 2.78 eV, when sulfur doping is applied, and when S-N-co doping is applied, it decreases from 2.97 to 2.63 eV. In addition, XRD analysis showed that some additional peak patterns were observed with S-N-codoped nanoparticles, which are the result of the partial transformation of complex compounds S and N. At the same time, the hexagonal structure of ZnO-NPs remains unchanged. The size of the NPs has been calculated using FWHM, and the size of N-S-dual-doped ZnO-NPs is smaller than that of single-doped and pure ZnO-NPs. ZnO-NPs with dual doping showed greater antimicrobial and antioxidant activity. Consequently, the dual-doped ZnO-NPs were much more effective than pure ZnO-NPs at inhibiting Gram-positive and Gram-negative bacteria species. Based on the results of this study, bandgap energy narrowing and surface-to-volume ratio increases can enhance the antimicrobial and antioxidant activity of ZnO-NPs. The improvement in antimicrobial is attributed to the improved stability and reduced particle size due to doping, which enables the particles to penetrate bacterial cell walls easily. This changes the structure of the cytoplasmic membrane, which in turn ruptures organelles and even leads to cell lysis. Doping of ZnO-NPs increases their antioxidant properties (from 52.45% to 88.94%) as well. Thus, such doped nanoparticles are ideal candidates for targeted delivery in vivo, combating oxidative stress [44].

Data Availability

The data used to support the findings of this study are included within the article.

Conflicts of Interest

The authors declare that they have no conflicts of interest.

Authors' Contributions

Diriba Yadesa, Jabessa Nagassa, and Tamene Tadesse Beyene conceived and designed the experiments, performed the experiments, and analyzed and interpreted the data; Diriba Yadesa and Tamene Tadesse Beyene wrote the paper; and Tamene Tadesse Beyene contributed reagents, materials, and analysis tools or data.

Acknowledgments

The authors express their gratitude for the financial support provided by Jimma University, Ethiopia.

References

[1] H. L. Kagdada, A. K. Bhojani, and D. K. Singh, "An overview of nanomaterials: history, fundamentals, and applications," in *Nanomaterials: Advances and Applications*, D. K. Singh, S. Singh, and P. Singh, Eds., pp. 1–26, Springer Nature Singapore, Singapore, 2023.

[2] P. N. Sudha, K. Sangeetha, K. Vijayalakshmi, and A. Barhoum, "Chapter 12- Nanomaterials history, classification, unique properties, production and market," in *Emerging Applications of Nanoparticles and Architecture Nanostructures*, A. Barhoum and A. S. H. Makhlouf, Eds., pp. 341–384, Elsevier, Amsterdam, Netherlands, 2018.

[3] H. F. Etefa, D. J. Nemera, and F. B. Dejene, "Green synthesis of nickel oxide NPs incorporating carbon dots for antimicrobial activities," *ACS Omega*, vol. 8, no. 41, pp. 38418–38425, 2023.

[4] J. Wang, X. Mu, M. Sun, and T. Mu, "Optoelectronic properties and applications of graphene-based hybrid nanomaterials and van der Waals heterostructures," *Applied Materials Today*, vol. 16, pp. 1–20, 2019.

[5] U. H. Naveed, N. Ayesha, U. Akhtar et al., "Synthesis approaches of zinc oxide nanoparticles: the dilemma of ecotoxicity," *Journal of Nanomaterials*, vol. 2017, Article ID 8510342, 14 pages, 2017.

[6] A. B. Tegenaw, A. A. Yimer, and T. T. Beyene, "Boosting the photocatalytic activity of ZnO-NPs through the incorporation of C-dot and preparation of nanocomposite materials," *Heliyon*, vol. 9, no. 10, Article ID e20717, 2023.

[7] O. V. Salata, "Applications of nanoparticles in biology and medicine," *Journal of Nanobiotechnology*, vol. 2, no. 1, p. 3, 2004.

[8] A. Ali Salman, "Application of nanomaterials in environmental improvement," in *Nanotechnology and the Environment*, S. Mousumi, Ed., IntechOpen, Rijeka, Croatia, 2020.

[9] K. W. Aga, M. T. Efa, and T. T. Beyene, "Effects of sulfur doping and temperature on the energy bandgap of ZnO nanoparticles and their antibacterial activities," *ACS Omega*, vol. 7, no. 12, pp. 10796–10803, 2022.

[10] D. J. Nemera, H. F. Etefa, V. Kumar, F. B. Dejene, and B. Francis, "Hybridization of nickel oxide nanoparticles with carbon dots and its application for antibacterial activities," *Luminescence*, vol. 37, no. 6, pp. 965–970, 2022.

[11] T. Naseem and T. Durrani, "The role of some important metal oxide nanoparticles for wastewater and antibacterial applications: a review," *Environmental Chemistry and Ecotoxicology*, vol. 3, pp. 59–75, 2021.

[12] Y. Yoon, P. L. Truong, D. Lee, and S. H. Ko, "Metal-oxide nanomaterials synthesis and applications in flexible and

wearable sensors," *ACS Nanoscience Au*, vol. 2, pp. 64–92, 2022.

[13] M. S. Chavali and M. P. Nikolova, "Metal oxide nanoparticles and their applications in nanotechnology," *SN Applied Sciences*, vol. 1, no. 6, p. 607, 2019.

[14] S. Jha, R. Rani, and S. Singh, "Biogenic zinc oxide nanoparticles and their biomedical applications: a review," *Journal of Inorganic and Organometallic Polymers and Materials*, vol. 33, no. 6, pp. 1437–1452, 2023.

[15] J. Jiang, J. Pi, and J. Cai, "The advancing of zinc oxide nanoparticles for biomedical applications," *Bioinorganic Chemistry and Applications*, vol. 2018, 18 pages, 2018.

[16] K. Davis, R. Yarbrough, M. Froeschle, J. White, and H. Rathnayake, "Band gap engineered zinc oxide nanostructures via a sol–gel synthesis of solvent-driven shape-controlled crystal growth," *RSC Advances*, vol. 9, no. 26, pp. 14638–14648, 2019.

[17] M. K. Debanath and S. Karmakar, "Study of blueshift of optical band gap in zinc oxide (ZnO) nanoparticles prepared by low-temperature wet chemical method," *Materials Letters*, vol. 111, pp. 116–119, 2013.

[18] M. Junaid, S. Ghulam Hussain, N. Abbas, and W. Q. Khan, "Band gap analysis of zinc oxide for potential bio glucose sensor," *Results in Chemistry*, vol. 5, Article ID 100961, 2023.

[19] S. Fiedler, L. C. Lem, C. Ton-That, M. Schleuning, A. Hoffmann, and M. R. Phillips, "Correlative study of enhanced excitonic emission in ZnO coated with Al nanoparticles using electron and laser excitation," *Scientific Reports*, vol. 10, no. 1, p. 2553, 2020.

[20] H. Agarwal, S. Venkat Kumar, and S. Rajeshkumar, "A review on green synthesis of zinc oxide nanoparticles – an eco-friendly approach," *Resource-Efficient Technologies*, vol. 3, no. 4, pp. 406–413, 2017.

[21] A. U. H. Khan, Y. Liu, R. Naidu, C. Fang, R. Dharmarajan, and H. Shon, "Interactions between zinc oxide nanoparticles and hexabromocyclododecane in simulated waters," *Environmental Technology and Innovation*, vol. 24, Article ID 102078, 2021.

[22] S. S. Naser, B. Ghosh, F. Z. Simnani et al., "Emerging trends in the application of green synthesized biocompatible ZnO nanoparticles for translational paradigm in cancer therapy," *Journal of Nanotheranostics*, vol. 4, pp. 248–279, 2023.

[23] S. Baruah and J. Dutta, "Effect of seeded substrates on hydrothermally grown ZnO nanorods," *Journal of Sol-Gel Science and Technology*, vol. 50, no. 3, pp. 456–464, 2009.

[24] A. Khalid, P. Ahmad, A. Khan et al., "Effect of Cu doping on ZnO nanoparticles as a photocatalyst for the removal of organic wastewater," *Bioinorganic Chemistry and Applications*, vol. 2022, Article ID 9459886, 12 pages, 2022.

[25] M. Carofiglio, S. Barui, V. Cauda, and M. Laurenti, "Doped zinc oxide nanoparticles: synthesis, characterization and potential use in nanomedicine," *Applied Sciences*, vol. 10, p. 5194, 2020.

[26] P. Porrawatkul, P. Nuengmatcha, A. Kuyyogsuy, R. Pimsen, and P. Rattanaburi, "Effect of Na and Al doping on ZnO nanoparticles for potential application in sunscreens," *Journal of Photochemistry and Photobiology B: Biology*, vol. 240, Article ID 112668, 2023.

[27] T. C. Bharat, Shubham, S. Mondal, H. S. Gupta, P. K. Singh, and A. K. Das, "Synthesis of doped zinc oxide nanoparticles: a review," *Materials Today: Proceedings*, vol. 11, pp. 767–775, 2019.

[28] A. G. Kaningini, S. Azizi, N. Sintwa et al., "Effect of optimized precursor concentration, temperature, and doping on optical properties of ZnO nanoparticles synthesized via a green route using bush tea (athrixia phylicoides DC.) leaf extracts," *ACS Omega*, vol. 7, pp. 31658–31666, 2022.

[29] X. Q. Zhou, Z. Hayat, D. D. Zhang et al., "Zinc oxide nanoparticles: synthesis, characterization, modification, and applications in food and agriculture," *The Scientific World Journal*, vol. 11, p. 1193, 2023.

[30] A. Dar, R. Rehman, W. Zaheer, U. Shafique, and J. Anwar, "Synthesis and characterization of ZnO-nanocomposites by utilizing aloe vera leaf gel and extract of *Terminalia arjuna* nuts and exploring their antibacterial potency," *Journal of Chemistry*, vol. 2021, Article ID 9448894, 7 pages, 2021.

[31] S. Asadpour, A. Raeisi vanani, M. Kooravand, and A. Asfaram, "A review on zinc oxide/poly(vinyl alcohol) nanocomposites: synthesis, characterization and applications," *Journal of Cleaner Production*, vol. 362, Article ID 132297, 2022.

[32] B. N. Raju, K. Ramji, and V. S. R. K. Prasad, "Mechanical properties of glass fiber reinforced polyester ZnO Nano-Composites," *Materials Today: Proceedings*, vol. 2, no. 4-5, pp. 2817–2825, 2015.

[33] J. I. Hong, L. S. Schadler, R. W. Siegel, and E. Mårtensson, "Rescaled electrical properties of ZnO/low density polyethylene nanocomposites," *Applied Physics Letters*, vol. 82, no. 12, pp. 1956–1958, 2003.

[34] B. Kulyk, V. Kapustianyk, V. Tsybulskyy, O. Krupka, and B. Sahraoui, "Optical properties of ZnO/PMMA nanocomposite films," *Journal of Alloys and Compounds*, vol. 502, no. 1, pp. 24–27, 2010.

[35] A. Król-Górniak, V. Railean, P. Pomastowski et al., "Comprehensive study upon physicochemical properties of bio-ZnO NCs," *Scientific Reports*, vol. 13, no. 1, p. 587, 2023.

[36] D. Kaur, A. Bharti, T. Sharma, and C. Madhu, "Dielectric properties of ZnO-based nanocomposites and their potential applications," *International Journal of Optics*, vol. 2021, pp. 1–20, 2021.

[37] J. Cui, "Zinc oxide nanowires," *Materials Characterization*, vol. 64, pp. 43–52, 2012.

[38] F. S. Hashim, A. F. Alkaim, S. J. Salim, and A. H. O. Alkhayatt, "Effect of (Ag, Pd) doping on structural, and optical properties of ZnO nanoparticales: as a model of photocatalytic activity for water pollution treatment," *Chemical Physics Letters*, vol. 737, Article ID 136828, 2019.

[39] S. G. Firisa, G. G. Muleta, and A. A. Yimer, "Synthesis of nickel oxide nanoparticles and copper-doped nickel oxide nanocomposites using phytolacca dodecandra L'herit leaf extract and evaluation of its antioxidant and photocatalytic activities," *ACS Omega*, vol. 7, no. 49, pp. 44720–44732, 2022.

[40] R. Abbasi, G. Shineh, M. Mobaraki, S. Doughty, and L. Tayebi, "Structural parameters of nanoparticles affecting their toxicity for biomedical applications: a review," *Journal of Nanoparticle Research*, vol. 25, no. 3, p. 43, 2023.

[41] S. F. U. Farhad, M. A. Hossain, N. I. Tanvir et al., "Structural, optical, electrical, and photoelectrochemical properties of cuprous oxide thin films grown by modified SILAR method," *Materials Science in Semiconductor Processing*, vol. 95, pp. 68–75, 2019.

[42] M. R. Islam, M. Rahman, S. F. U. Farhad, and J. Podder, "Structural, optical and photocatalysis properties of sol–gel deposited Al-doped ZnO thin films," *Surfaces and Interfaces*, vol. 16, pp. 120–126, 2019.

[43] J. Kong, S. Zhang, M. Shen, J. Zhang, and S. Yoganathan, "Evaluation of copper(I)-doped zinc oxide composite nanoparticles on both gram-negative and gram-positive bacteria," *Colloids and Surfaces A: Physicochemical and Engineering Aspects*, vol. 643, Article ID 128742, 2022.

[44] B. C. Ghos, S. F. U. Farhad, M. A. M. Patwary et al., "Influence of the substrate, process conditions, and postannealing temperature on the properties of ZnO thin films grown by the successive ionic layer adsorption and reaction method," *ACS Omega*, vol. 6, no. 4, pp. 2665–2674, 2021.